Journal of Catalysis 363 (2018) 128–135

Contents lists available at ScienceDirect

Journal of Catalysis

journal homepage: www.elsevier.com/locate/jcat

Quality control for Ziegler-Natta catalysis via spectroscopic fingerprinting

Paul Pletcher [a], Alexandre Welle [b], Aurélien Vantomme [b], Bert M. Weckhuysen [a,*]

[a] Inorganic Chemistry and Catalysis, Debye Institute for Nanomaterials Science, Utrecht University Universiteitsweg 99, 3584CG Utrecht, The Netherlands
[b] Total Research and Technology Feluy, Zone Industrielle C, B-7181 Seneffe, Belgium

ARTICLE INFO

Article history:
Received 4 February 2018
Revised 31 March 2018
Accepted 9 April 2018
Available online 7 May 2018

Keywords:
Spectroscopy
FTIR
UV–Vis
Ziegler-Natta
Polyethylene
Structure-Performance

ABSTRACT

Commercial olefin polymerization catalysts are typically produced at a manufacturing site before transport to production facilities for storage and eventual use. During transport and storage, catalysts can deteriorate resulting in decreased catalytic performance due to contact with environmental factors. In this work, a spectroscopic toolbox was developed for quality assurance purposes of a third generation Ziegler-Natta catalyst for ethylene polymerization. A pre-activated, industrial Ziegler-Natta catalyst was exposed singly to heat, dry air, and moisture to study the specific environmental factors. Activity tests were performed with the polymer morphology inspected by SEM and image analysis. Catalyst characterization was conducted using Fourier Transform Infrared spectroscopy with CO and Diffuse Reflectance UV–Vis spectroscopy to relate unique spectroscopic fingerprints to different environmental effects. Reactivity towards gas-phase ethylene polymerization was tested using Diffuse Reflectance Infrared Fourier Transform spectroscopy. This work demonstrates the development of a new spectroscopic methodology useful for quality control in Ziegler-Natta catalysis.

© 2018 Elsevier Inc. All rights reserved.

1. Introduction

Although one of the industrial workhorses for the generation of isotactic polypropylene, the Ziegler-Natta (ZN) catalyst remains an important catalyst for the production of high density polyethylene (HDPE) [1,2]. The third generation ZN catalyst, consisting of atomically dispersed $TiCl_4$ on the (1 0 4) and (1 1 0) defect planes of a spherical $MgCl_2$ support, is activated by addition of an organoaluminum cocatalyst, typically triethylaluminum (TEA), and lacks the additional internal donors used for isotactic polypropylene production. Activation of the ZN catalyst with TEA generates a variety of atomically dispersed Ti(II) and Ti(III) species containing three to five ligands, these ligands comprised of a mixture of chloride and ethyl ligands, and one to three open vacancies [3–7]. Furthermore, small clusters of reduced $Ti(III)_XCl_Y$ have been known to form during the interaction with TEA [3–9]. Of these species, a 5-coordinated Ti(III) atom anchored to the (1 1 0) plane featuring an ethyl ligand and an open coordination site is widely considered to be the active site for olefin polymerization, although catalyst sites containing Ti(II) have also been proposed for ethylene polymerization [8,9]. The spherical-shaped morphology for the support is also crucial for reliable post-catalysis polymer processing as the final HDPE particle retains the original catalyst shape post polymerization [4,5,10–16].

Due to the reactivity of the material components, the fully activated ZN catalyst is sensitive to environmental factors, such as moisture, oxygen, heat, and light, that can lead to catalyst degradation i.e. oxidation of reduced Ti species to Ti(IV). While some of these factors may be mitigated by activating the catalyst immediately before polymerization, this remains a concern as some HDPE production lines rely on fully activated ZN catalysts generated at the catalyst production site. These fully activated catalyst are then shipped and stored at the chemical plant, allowing for the possibility of catalyst deterioration due to improper storage. While formation of HDPE with a consistent spherical shape is important for postproduction processing, non-ideal morphologies such as polyethylene "threads" produce inferior polymer products and can result in unwanted reactor fouling [4,5,10,11]. It is therefore imperative for industrial actors to have access to diagnostic tools to predict a catalyst's performance for quality control purposes before use on the industrial scale.

Our goal is to develop such a diagnostic toolkit to understand catalyst structure as related with catalytic performance and polymer morphology for a series of deteriorated ZN catalysts. To this end, a third generation ZN catalyst, not containing internal donors, was synthesized and activated using TEA. Portions of this activated

* Corresponding author.
E-mail address: b.m.weckhuysen@uu.nl (B.M. Weckhuysen).

https://doi.org/10.1016/j.jcat.2018.04.012
0021-9517/© 2018 Elsevier Inc. All rights reserved.

catalysts were then singly exposed to dry air, moisture, or an extended heat treatment to simulate deterioration for different environmental conditions. Activity experiments were conducted using industrial conditions and the morphology of polymer products analyzed using Scanning Electron Microscopy (SEM) and image analysis. The catalysts were characterized using Fourier Transform Infrared (FT-IR) spectroscopy with CO as a probe molecule to study Lewis acidity. Diffuse Reflectance Ultraviolet–Visible (DR UV–Vis) spectroscopy was used to study the oxidation state of Ti species. Ethylene reactivity experiments were monitored using Diffuse Reflectance Infrared Fourier Transform spectroscopy (DRIFTS).

2. Experimental

2.1. Materials and conditions

Anhydrous 99% $MgCl_2$, TEA, heptane, and 99% KBr were purchased from Sigma and was used as such. 15% CO balance Ar, 3.5 Ethylene, 4.0 Oxygen, and 6.0 Nitrogen gas cylinders were purchased from Linde Gas Group. Unless otherwise stated, all manipulations were conducted in N_2 inert atmospheres using gloveboxes or Schlenk techniques.

2.2. Catalyst preparation

All materials were produced using air and water free conditions. ZN catalyst C_{AsSuch} was prepared according to literature procedure [17] with the chemical synthesis by the addition of increasing amounts of chlorinating agents (i.e. $ClTi(OR)_3$) to a magnesium alkoxide solution in heptane. Addition of $TiCl_4/TiOR_4$ mixtures and a final addition of $TiCl_4$ generated the solid, spherically titanated catalyst. The active catalyst, C_{AsSuch}, was then activated with TEA, filtered, dried, and stored under inert atmosphere away from light. No internal donors were used for the catalyst preparation. The dry air treated catalyst, $C_{DryAir,}$ was prepared by stirring a portion of the C_{AsSuch} catalyst in dry, oxygenated heptane for 24 h at room temperature before solvent removal. The moisture treated sample, $C_{Moisture}$, was prepared by stirring a portion of the C_{AsSuch} in water-saturated, deoxygenated heptane for 24 h before solvent removal. The heat-treated sample, C_{Heat} ,was prepared by storing a portion of the dry, powdered C_{AsSuch} catalyst under an inert atmosphere in an oven at 323 K for 5 days away from light.

2.3. Activity testing

2.3.1. Ethylene polymerization via autoclave

Polymerization reactions were performed in a 4 L autoclave with an agitator, a temperature controller, and inlets for feeding of ethylene and hydrogen. The reactor was dried at 403 K with N_2 for one hour and then cooled to 313 K.

The reactor was loaded with 2 L of isobutane, 6 wt% of 1-hexene, 120 ppm of TEA as a scavenger, 0.2 mol of H_2, and pressurized with ethylene to 23.4 bar. Polymerization started upon catalyst injection (5 mg), was performed at 358 K and was stopped after 60 min by reactor depressurization. Reactor was flushed with nitrogen prior opening and the polymer was dried at 323 K overnight under reduced pressure.

2.4. Characterization methods

2.4.1. Catalyst composition

Elemental composition of dried C_{AsSuch} samples were determined by ICP-MS analysis to contain an 8.0% weight loading of Ti.

2.4.2. Surface area determination

N_2 physisorption isotherms were measured to determine surface areas and pore volumes using a Micromeritics Tristar 3000 setup. The samples were outgassed at room temperature for 1 h prior to performing the measurements at liquid nitrogen temperature. Surface areas were determined using the Brunauer – Emmett–Teller (BET) theory.

2.4.3. SEM

Polymer samples were deposited on a double face adhesive carbon tape, and then metalized with platinum.

2.4.4. Polymer sphericity via image analysis

Polymer samples were analyzed using a Retsch Technology® Camsizer® to study the particle morphology. Free flowing polymer powder entered through a DR100-75 RT metering feeder and a high-speed camera photographed individual particles as they passed in front of the camera. Analysis of the digital images determined the two-dimensional area and an average circumference of the particles. The ratio of the two-dimensional area to the square of the average circumference value was multiplied by a constant, 4π, to determine a sphericity value. For a perfect sphere, the sphericity value equals 1. Deviations from the spherical shape produce smaller values that asymptotically approach zero.

2.4.5. FT-IR spectroscopy with a CO probe

A pellet was prepared inside of an inert, N_2 atmosphere glovebox using a hand press. Pellets of 10.0 ± 0.2 mg were prepared from premade catalysts to allow for quantitative comparison between catalyst samples. The pellets were loaded into a specialty transmission IR cell fitted with CaF_2 windows in a glovebox. Spectra were taken using a Perkin-Elmer 2000 instrument using 32 scans at a resolution of 4 cm^{-1}. The sealed cell was connected to a gas delivery and vacuum system, evacuated carefully to prevent interaction with air/moisture, and cooled with liquid nitrogen to 87 K. The sample was then dosed with increasing amounts of CO at 87 K until the sample was saturated, 15 mbar.

2.4.6. DR UV–Vis spectroscopy

Samples were loaded inside of an inert atmosphere glovebox into 0.20 ml quartz cuvettes with a sealable cap. Spectra were taken with an Avantes DR UV–Vis probe spectrometer held at an angle to the quartz cuvette to prevent direct reflection from the probe. Anhydrous $MgCl_2$ was used as a blank.

2.4.7. Polymerization via DRIFTS

DRIFTS measurements were taken on a Perkin-Elmer instrument fit with a MCT detector. An air-free Harrick Praying Mantis high temperature reaction cell was used to conduct all ethylene polymerization measurements. A background was taken using finely ground KBr. The cell was then loaded inside an inert atmosphere glovebox with roughly 40.0 mg of catalysts powder and closed to prevent interaction with water or oxygen. The cell was connected to the spectrometer and the lines flushed with 6.0 Nitrogen for 20 min before switching to an ethylene flow of 5 ml/min. During this time, the sample was heated to the reaction temperature of 358 K. After reaching the required temperature, spectra were taken of 32 scans at a resolution of 4 cm^{-1} were taken every minute and the ethylene gas flow was directed through the cell. Reactions were monitored until polymer signal saturation or for 2 h, depending which occurred first.

Table 1
Overview of the catalytic performance and related polymer morphology as obtained for the pristine and deactivated Ziegler-Natta catalyst under study.

Catalyst	Activity[a,b]	Threads[c]	SPHT
C_{AsSuch}	1	No	0.80
C_{DryAir}	0.82	Yes	0.21
$C_{Moisture}$	0.75	Yes	0.52
C_{Heat}	0.70	Yes	0.66

[d]Sphericity as determined by image analysis of the catalyst particles. SPHT values fall in the range of 1–0, with a value of 1 representing a perfect sphere and values closer to 0 showing greater deviation from a spherical shape.
[a] Conditions: 2 L isobutane as a solvent; reaction at 358 K; 120 ppm TEA as a scavenger; 0.1 mol of H_2; 23.4 bar pressure ethylene for 1 h in a 4 L reactor.
[b] Values normalized to C_{AsSuch} activity.
[c] As determined by SEM.

3. Results and discussion

3.1. Ethylene activity testing under industrial conditions

To understand the effects of environmental factors, a catalyst library was studied based on an chemically synthesized industrial ZN catalyst, labeled C_{AsSuch}, containing 8.0% weight loading of Ti. This catalyst library included the TEA activated C_{AsSuch} and portions of the prepared C_{AsSuch} catalyst exposed to dry air, moisture, or heat. The deteriorated catalysts were denoted as C_{DryAir}, $C_{Moisture}$, and C_{Heat}, respectively. As the catalyst stock was a third generation ZN catalyst, none of the samples contained internal donors. Polyethylene activity tests were conducted and the produced HDPE examined for threading and particle sphericity (SPHT). The results are summarized in Table 1. As expected, the poisoned catalysts displayed reduced HDPE activity. The reactivity decreased in the order of $C_{AsSuch} > C_{DryAir} > C_{Moisture} > C_{Heat}$. Surprisingly, the overall reactivity was comparable, showing less than a factor of 2 difference between the most and least active catalysts. The HDPE prepared from C_{AsSuch} showed an ideal spherical-like morphology, as shown in Fig. 1A. However, all poisoned catalysts exhibited undesirable polymer morphologies with the appearance of polymer threads when analyzed using SEM, as illustrated in Fig. 1B. Quantitative analysis of the polymer morphology was utilized via image analysis using a Camsizer® instrument. The poisoned catalysts showed significant deviations in particle sphericity, with decreasing spherical morphology in the order of $C_{AsSuch} > C_{Heat} > C_{Moisture} > C_{DryAir}$. The differences in HDPE activity and polymer morphology between deteriorated catalysts and C_{AsSuch} suggest unique spectroscopic features found in the different ZN catalysts could be used to discriminate between deteriorated catalysts for quality control purposes.

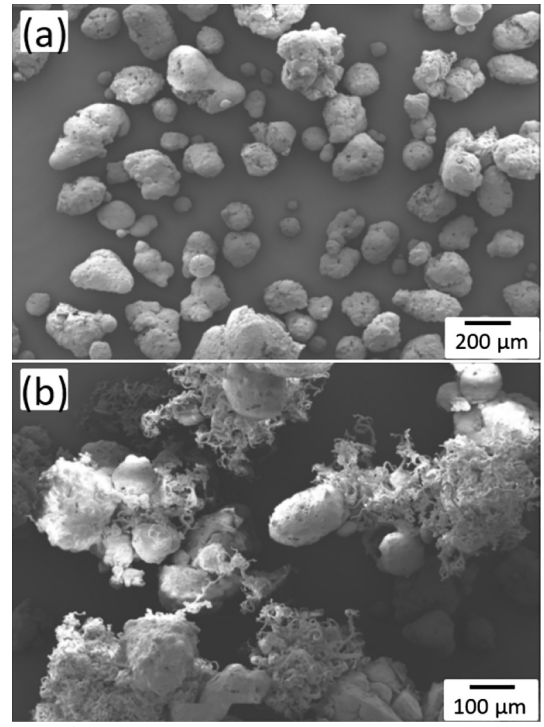

Fig. 1. SEM of (a) HDPE with ideal morphology and (b) HDPE with threads as obtained with respectively C_{AsSuch} and C_{heat}.

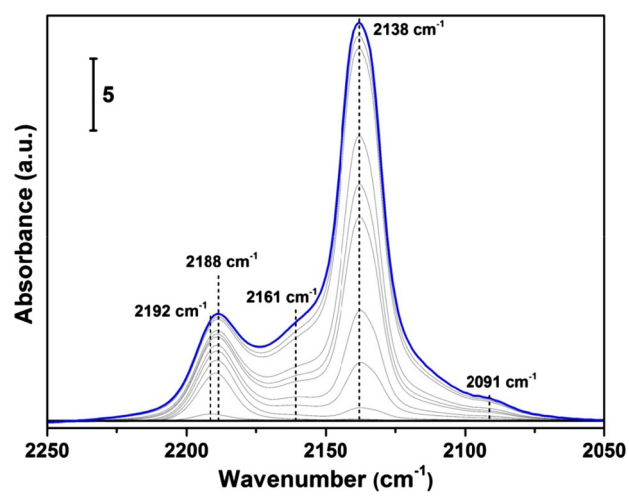

Fig. 2. Difference FT-IR Spectra for CO adsorption of C_{AsSuch} at 87 K with increasing CO pressure. The initial spectrum is shown in black, intermediate spectra in grey, and the final spectrum at CO saturation, 15 mbar, is in blue. The four CO adsorption bands correspond to physically adsorbed CO at 2138 cm^{-1}, CO adsorbed to 5-coordinate Mg(II) at 2161 cm^{-1}, CO adsorbed on 4-coordinate Mg(II) at 2192 cm^{-1} that red-shifts to 2188 cm^{-1} at high CO coverage, and a band at 2091 cm^{-1} for CO adsorbed to Ti(III).

3.2. Characterizing the Lewis acidity of catalysts via CO FT-IR spectroscopy

To study the effect of environmental factors on the catalyst structure, FT-IR studies were conducted. The Mid-IR spectra shown in Fig. S1 only revealed minor differences, except in the case of $C_{Moisture}$ which showed an overwhelming presence of water. To study the acidity of the different catalysts, CO was used as a probe molecule, similarly to previous literature reports on heterogenized metallocene catalysts [18,19]. The CO adsorption FT-IR spectra for C_{AsSuch} is shown in Fig. 2. This spectrum is representative of the CO FT-IR studied for the prepared catalysts. CO adsorption spectra for the degraded samples are included as Figs. S2–S5. The CO bands appear only at low temperature and disappeared with evacuation or increasing temperature. This demonstrates the presence of weakly bonded CO to Lewis acid sites on the catalyst. An exception was found in the case of $C_{Moisture}$, Fig. S4, which showed no gas adsorption on the catalyst sample, even at low temperature. To probe the surface, the $C_{Moisture}$ sample was heated under vacuum at 373 K in the FT-IR cell for 1 h before CO dosing at 87 K, Fig. S5, and is labeled as $C_{MoistureDried}$.

With increased dosing of CO at 87 K, adsorption studies of catalyst C_{AsSuch} exhibited several bands between 2250 cm^{-1} to 2050 cm^{-1}. The catalyst is shown to have a pore network as characterized by the 2138 cm^{-1} band for liquid-like CO enclosed in a confined space [18–21]. The FT-IR bands at 2188 cm^{-1} and 2161 cm^{-1}, at high CO coverage, are assigned to CO bound to

4-coordinate and 5-coordinate Mg(II), as previously reported for de-alcoholated $MgCl_2$ [22]. Specifically, the 2188 cm^{-1} band can be assigned to Mg(II) atoms exposed on (1 1 0) or (0 1 5) surfaces and the 2161 cm^{-1} band assigned to Mg(II) at (1 0 4). The 2188 cm^{-1} band initially appeared at 2192 cm^{-1} and underwent a redshift with increasing CO coverage, caused by neighboring CO molecules interacting with one another as coupled oscillators [22]. However as the bands for CO adsorbed onto 4-coordinate Mg(II) sites only shift minimally with increased CO coverage, this suggests that the support in C_{AsSuch} is comprised of small crystallites lacking an extended surface or that the high coverage of Ti species disrupts the interaction of adsorbed CO molecules on the surface. The band at 2091 cm^{-1} is tentatively assigned to Ti(III) based on literature reports for organometallic, Ti(III) metallocene compounds reported in the 2080–2020 cm^{-1} range [23]. The observed blue shift may be the result of the more polarizing environment around the Ti atom due to the coordination of four chlorine ligands to the metal center, as compared to the organometallic Ti(III) complexes. Interestingly, the band intensity for the Ti(III) seem comparable for C_{AsSuch} and C_{DryAir}.

Comparing C_{AsSuch} with the modified catalysts at a saturation pressure of 15 mbar revealed significant differences in terms of catalyst porosity, Mg(II) Lewis acidity, and Ti(III) sites, as illustrated in Fig. 3. While the spectrum of C_{DryAir} shows a similar intensity for the band at 2138 cm^{-1} (associated with physically adsorbed CO), there are subtle changes in the relative intensity of the bands associated to CO coordinated to the 4- and 5-coordinate Mg(II) cations. The C_{DryAir} sample shows an increase in the band associated with the 5-coordinate Mg(II) sites and a slight redshift to 2159 cm^{-1}, compared to 2161 cm^{-1} band of the pristine sample. Additionally, the C_{DryAir} sample exhibits a decrease in the band associated with 4-coordinate Mg(II) sites and a redshift from 2188 cm^{-1} to 2185 cm^{-1}. These shifts in the bands represent CO bonded to Mg(II) may relate to conditions on the support surface. Measurements on the catalyst surface areas, Table S1, revealed relatively large changes to the catalyst surface, depending on the type of environmental influence. Surprisingly, the heat treatment to the pristine catalyst led to an increase in surface area while the interaction with oxygen or water, unsurprisingly, led to a decrease in surface area due to subsequent changes to the $MgCl_2$ surface. The decrease in surface area for $C_{Heat} > C_{AsSuch} > C_{DryAir} > C_{Moisture}$ follows the same pattern for the shift in the 4-coordinate Mg(II) band, C_{Heat} (2190 cm^{-1}) > C_{AsSuch} (2188 cm^{-1}) > C_{DryAir} (2185 cm^{-1}) and suggests that the bands shift with decreasing surface area. Lack of CO coordination to 4-coordinate Mg(II) for the moisture treated sample may mean water strongly coordinated to these sites or has reorganized the support surface.

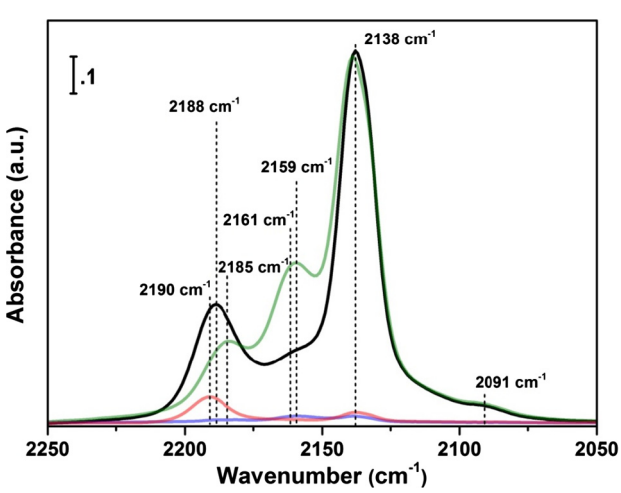

Fig. 3. Comparison of difference FT-IR spectra for 15 mbar CO at 87 K with C_{AsSuch} in black, C_{Heat} in red, C_{DryAir} in green, and $C_{MoistureDried}$ in blue. Bands for CO adsorption correspond to Mg(II) sites at 2200–2160 cm^{-1}, pores for physically adsorbed CO sites at 2138 cm^{-1}, and Ti(III) sites at 2091 cm^{-1}.

The catalyst surface area measurements, as compared to the quantitative CO FTIR, do require additional comment as the results seem counterintuitive between C_{Heat} and C_{DryAir} – the higher surface area catalyst C_{Heat} exhibits very little CO adsorption while the lower surface area catalyst C_{DryAir} has similar CO adsorption to the pristine, C_{AsSuch} catalyst. While these changes to the $MgCl_2$ surface are difficult to rationalize, it is possible that the heat treatment may have caused a reorganization of the (1 1 0) and (1 0 4) planes in the $MgCl_2$ surface without reduction in surface area. Additionally, the influence of oxygen may have caused limited reorganization of the $MgCl_2$ (1 1 0) and (1 0 4) surfaces but lead to the degradation of species on the catalyst surface and reduce the higher surface are of C_{AsSuch}. Such features will be examined in Section 3.2.

For catalysts C_{Heat} and $C_{MoistureDried}$, the CO adsorption showed dramatic changes to the catalysts with significant losses in support porosity, Mg(II) sites, and Ti(III) sites. The 4-coordinate Mg(II) sites for the C_{Heat} sample undergo a blue shift to 2190 cm^{-1}, suggesting that the 4-coordinate Mg(II) sites are more isolated and do not exhibit the same coupled oscillator effect seen with C_{AsSuch}. For the $C_{MoistureDried}$ sample, there is comparably fewer Mg(II) sites and lacks the porosity of the pristine sample. Furthermore, studying the $C_{MoistureDried}$ spectrum in Fig. S5, revealed CO bands commonly associated with TiO_2 and Al_2O_3 type structures [24–27]. When comparing CO FT-IR studies with the bulk activity studies from Table 1, there appears to be a structure-activity relationship between the deteriorating effects of heat and moisture to the Lewis acidity of the catalyst surface and observed polymerization activity. While moisture is a known poison for the ZN catalyst, it was surprising to note that extended exposure to heat caused similar levels of surface deterioration.

The CO band seen at 2091 cm^{-1} is of interest as the interaction of CO with the Ti(III) site for ZN catalyst systems have not been studied in detail. Due to the broad shift in the 2075 cm^{-1} to 2120 cm^{-1} region, the C_{AsSuch} and C_{DryAir} spectra from Fig. 3 were deconvoluted and the Ti(III) bands analyzed, Figs. S6, S7 and Tables 2S–3S, using Fityk software [28]. However, these results should be considered carefully as the natural abundance of ^{13}CO overlaps with the potential Ti(III)-CO band. After a subtracting the ^{13}CO overlaying bands and band deconvolution, C_{AsSuch} and C_{DryAir} were revealed to have small bands at 2098 cm^{-1} and 2091 cm^{-1}, respectively. The shift between the two samples may be due to differences in the support surface or coordination environment of the Ti(III) species. Interestingly, the deconvolution reveals that the C_{AsSuch} sample has almost twice as much Ti(III)-CO coordination as compared to the C_{DryAir} catalyst with band areas of 0.25–0.14, respectively. Again, these results should be considered carefully, due to the difficulty in band deconvolution. Further implications will be discussed in Section 3.2.

3.3. Characterizing Ti oxidation states using DR UV–Vis spectroscopy

As a method of determining oxidation states, DR UV–Vis spectroscopy has been instrumental in identifying different metal species in supported metal oxide catalysts [7,29–31]. This technique was applied to distinguish the effect of the different environmental conditions on the Ti oxidation states and is shown in Fig. 4. The spectrum for C_{AsSuch} revealed a diverse array of Ti species. The bands at 32,000 cm^{-1}, 36,100 cm^{-1}, and at higher wavenumbers are representative of intense Ligand to Metal Charge Transfers (LMCT) for the different Ti species [31]. The band at 26,900 cm^{-1} is indicative of inter-site charge transfers between reduced Ti

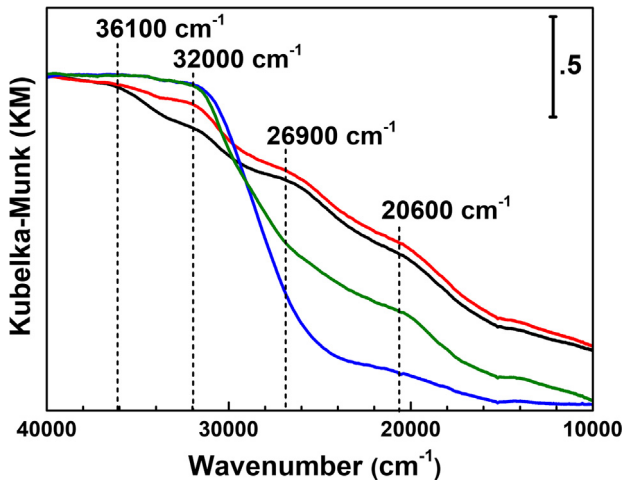

Fig. 4. DR UV–Vis spectra for C_{AsSuch} in black, C_{Heat} in red, C_{DryAir} in green, and $C_{Moisture}$ in blue. Bands at 32,000 cm^{-1}, 36,100 cm^{-1}, and above represent the LMCT region. 26,900 cm^{-1} is indicative for d-d intersite transfers for Cl-bridged, reduced Ti clusters. Region between 23,000 cm^{-1} to 10,000 cm^{-1} represent the d-d electronic transitions with a band at 20,600 cm^{-1}.

centers bridged by halide ligands, as reported in Ti(III) trihalides samples [32,33]. The bands between 22,500 cm^{-1} to 10,000 cm^{-1} are characteristic of reduced Ti(III) and Ti(II) species [31]. The broad bands in this region suggest that the Ti complexes exist in distorted octahedral environments due to the Jahn-Teller effect [32,33].

It has been observed that changing the environmental conditions have pronounced effects on the Ti oxidation state. For the C_{Heat} sample, the slight increase to the 32,000 cm^{-1} and MLCT band region suggest that some Ti species were re-oxidized to Ti(IV), although influences by the cell position affecting the band intensity cannot be ruled out. Most Ti species were unaffected and the spectrum from 30,000 cm^{-1} to 10,000 cm^{-1} is similar in shape to the C_{AsSuch} sample spectra. The increase in absorbance for the C_{Heat} sample, as compared with the C_{AsSuch} sample, between 30,000 cm^{-1} to 10,000 cm^{-1} may be the result of particle size effects or increased signal reflection as oppose to increases in concentration of reduced Ti signals. C_{DryAir} exhibited oxidation to potentially half of all Ti(II) and Ti(III) species, in comparison to the UV–Vis signal of C_{AsSuch}, and complete loss of the d-d inter-site transfers unique to reduced Ti clusters. The oxidation and rearrangement of these Ti_x-Cl_y clusters may explain why the C_{DryAir} catalyst exhibited a lower surface area as compared to the C_{AsSuch}, despite showing similar concentrations of adsorbed CO. $C_{Moisture}$ showed dramatic oxidative changes and the conversion of nearly all Ti(II) and Ti(III) species to Ti(IV), although some reduced Ti species remain unaffected.

A tentative reaction scheme, Scheme 1, is shown to suggest potential Ti species generated from C_{AsSuch} from exposure to dry air or moisture. The active site (A) is expected to be an Ti(III) atom, featuring an ethyl ligand, anchored to the (1 1 0) $MgCl_2$ surface. However, as C_{AsSuch} represents an aged catalyst, it is possible that the sensitive Ti(III)-Ethyl bond may degrade into Ti(III)-H, (B), and ethylene, as reported for similar homogeneous Ti(III)-R compounds at room temperature [34]. However, reports concerning Ti(III)-R species anchored onto heterogeneous supports by Nesterov et al. and Maksimov et al. showed that only a fraction of Ti (III)-Ethyl species decomposed to form Ti(III)-H, even after heating at 100 Celsius for 1 h. This suggests that heterogeneous Ti(III)-R species may be far more stable than their homogeneous counterparts [35,36]. They found the appearance of Ti(III)-H species produced a new band at 1560 cm^{-1}, representing the Ti(III)-H stretching [35,37,38]. Examination of the Mid-IR region of C_{AsSuch} in Fig. 1S showed a minor band at 1560 cm^{-1}, signifying only a minor faction of (A) is converted into (B). Regardless, these species, as well as other Ti(III) and Ti(II) species, are expected to appear in the 30,000 cm^{-1} to 10,000 cm^{-1} region. Exposure of (A) or (B) to moisture is expected to induce hydrolysis to generate (C), which may constitute some of the remaining Ti(III) species observed in Fig. 4. Further hydrolysis should produce Titania and explain the spectra in Fig. S5 for signals similar to that of CO adsorbed on Titania. In contrast, the exposure of (A) to dry air may generate the Ti (IV) peroxo species (D) or (E), as previously reported [6]. Unfortunately, these Ti(III)-OH and Ti(IV) peroxo species are only speculative as their spectroscopic FTIR fingerprints are either found below 1000 cm^{-1}, outside the limit of the FTIR window material, or are masked by other intense bands, such as the presence of intense water bands concealing potential Ti(III)-OH bands in Fig. S1 for the $C_{Moisture}$ [39].

Taking into consideration the CO FT-IR information and previous literature reports, the DR UV–Vis spectra suggest unique pathways for catalyst deactivation, summarized in Fig. 5. The effect of dry air on the pristine catalyst preserved the porosity of the catalyst structure but oxidized potentially half of the Ti(II) and Ti(III) species to Ti(IV), particularly affecting $TiCl_3$ clusters. This correlates with the CO FT-IR band deconvolution results between C_{AsSuch} and $C_{DryAir.}$ This is further evidence that the band assigned to 2098 cm^{-1} to 2091 cm^{-1} is related to the Ti(III) active species as the UV–Vis results show oxidation of roughly half of the Ti(III) species and complete loss of the Ti clusters. Alternatively, exposing C_{AsSuch} to heat caused dramatic changes to the support structure and may have resulted in limited oxidation of some Ti species. Exposing the pristine catalyst to moisture led to formation of oxidized Ti and Al species and the elimination of pores.

3.4. Monitoring ethylene polymerization using DRIFTS

Due to the results of the ethylene activity experiments and the presence of reduced Ti species found in the DR UV–Vis studies, ethylene reactivity experiments were conducted in a DRIFTS cell to measure the rate of polymer formation. As shown previously, olefin polymerization can be monitored using DRIFTS to investigate the influence of catalyst structure on polymerization activity [40]. Exposing C_{AsSuch} to an ethylene flow of 5 ml/min at 358 K led to the rapid formation of polyethylene, as shown in Fig. 6a and Fig. 6d, with characteristic HDPE band stretching observed in both the $\nu(CH_2)$ and $\nu(CH)$ regions [24,40]. The asymmetric $\nu(CH_2)$ appear at 2926 cm^{-1} and the symmetric $\nu(CH_2)$ bands at 2852 cm^{-1}, as illustrated in Fig. 6b. Bands associated with crystalline and amorphous HDPE appeared at 1466 cm^{-1} and 1456 cm^{-1} are shown in Fig. 6c, respectively [24]. As the crystalline HDPE band intensity is greater than the intensity of the amorphous HDPE band, it is clear that C_{AsSuch} forms crystalline HDPE (see Fig. 6.).

Kinetic measurements for polymer formation were analyzed by following the band intensity growth of the symmetric $\nu(CH_2)$ stretch at 2852 cm^{-1}, as illustrated in Fig. 6e. The signal corresponds to the growth of the CH_2 signals from the first insertion of the ethylene into the ethyl group of the catalyst, known as initiation, and later, additional insertions of ethylene into the attached polymer, called propagation. This mechanism is known as the Cossee-Arlman mechanism [41–43], shown in Scheme S1. As the aged catalyst C_{AsSuch} does contain some Ti(III)-H sites, the active Ti(III)-Ethyl catalyst is expected to be reformed rapidly as olefin insertion into the metal-hydride bond [44,45]. This equilibrium in Scheme S1, K_f, is shifted to the right and should represent a fast reaction step not observed during the reaction [35,36,44,45]. Kinetic analysis of the olefin polymerization showed a slow initiation rate constant and a fast propagation rate constant, i.e., 0.147 min^{-1} and $\geq$16.314 min^{-1}, respectively. The propagation rate con-

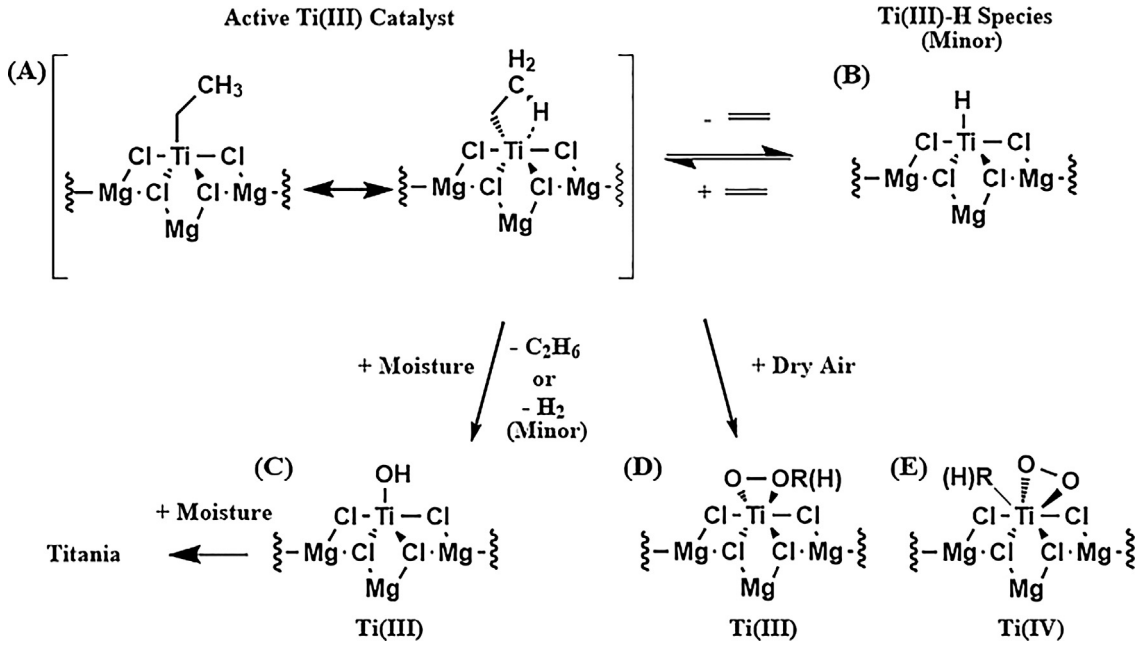

Scheme 1. Possible degradation of speculative Ti(III) active site as exposed to Moisture or Dry Air.

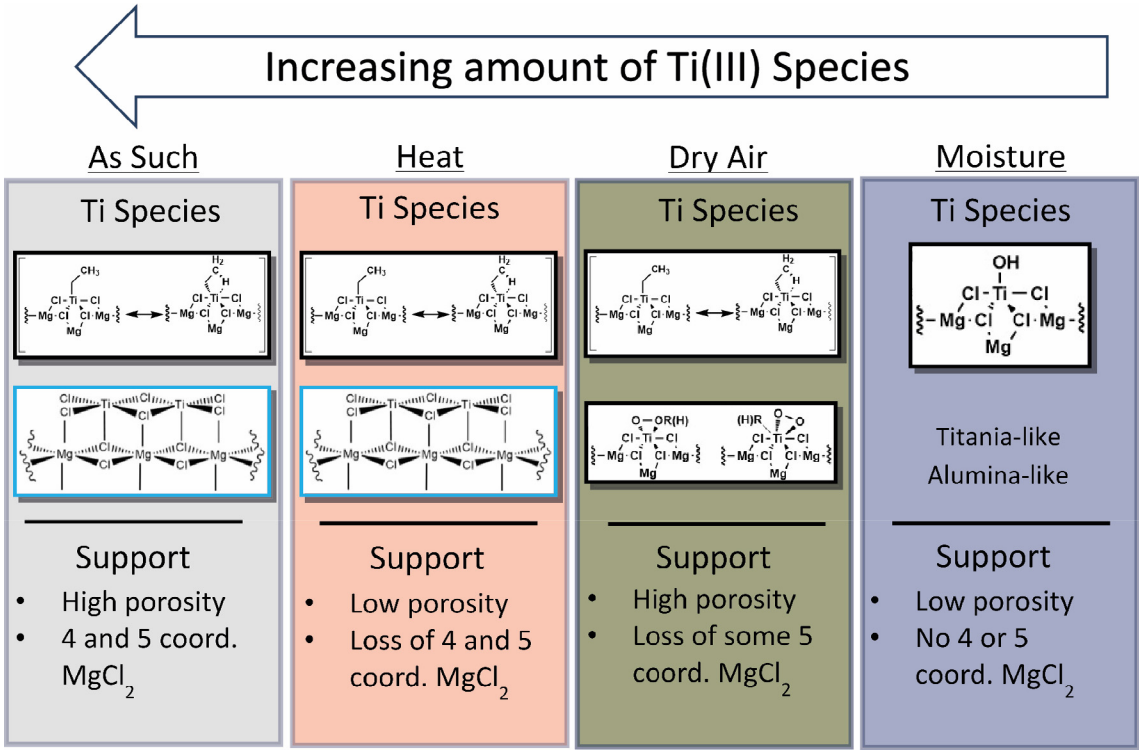

Fig. 5. Summary of the pristine and environmentally modified ZN catalyst structures, including the effect of the coordination environment of $MgCl_2$ and potential Ti species.

stant should only be taken as a minimum value as the polymer growth was extremely rapid and the collection of spectra at later time points became impossible due to HDPE signals overwhelming the detector. This indicates that the propagation step is at least 2 orders of magnitude faster than the initial ethylene insertion step. While previous studies have reported on the kinetics of polyethylene formation of ZN catalysts, the initiation rate is modelled as equivalent to the propagation rate [9,46]. However, literature on olefin polymerization for homogeneous group (IV) polymerization catalysts have reported k_p values as roughly 2 orders of magnitude larger in comparison to k_i, in agreement with the reported results [47,48]. Additionally, the formation of HDPE exhibited a smooth growth of polymer over time, in contrast to studies with silica based supports that require support fracturing over time [16]. This controlled growth step is reported to be crucial for the formation of polymer products with ideal morphology [11–14,49].

However, the DRIFTS experiments with the other catalyst structures, C_{Heat}, C_{DryAir}, and $C_{Moisture}$, did not result in polyethylene

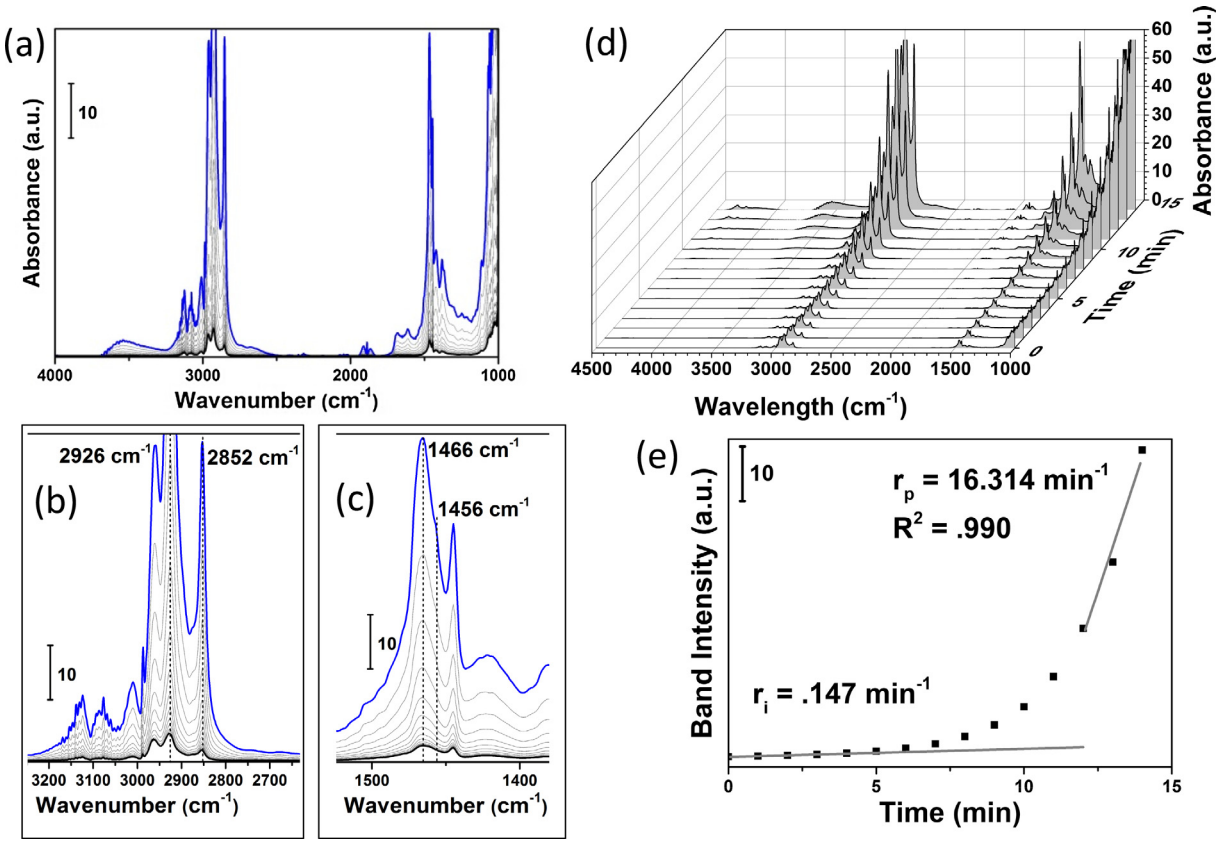

Fig. 6. DRIFT spectroscopy of ethylene polymerization for C_{AsSuch} at 358 K and 1 bar ethylene. (a) The initial spectrum is in black, intermediate spectra are in grey, and the final spectrum at 14 min is in blue with spectra taken every minute. (b) absorption band at 2926 cm^{-1} represents the asymmetric $\nu(CH_2)$ band, while the 2852 cm^{-1} band represents the symmetric $\nu(CH_2)$ band. (c) the 1466 cm^{-1} and 1456 cm^{-1} bands are related to the crystalline and amorphous phases of HDPE, respectively. (d) the time evolution of HDPE formation with the (e) kinetics of polymer growth was monitored using the increase in the symmetric $\nu(CH_2)$ 2852 cm^{-1} band intensity over time. Catalysts C_{DryAir}, $C_{Moisture}$, and C_{Heat} did not show ethylene reactivity under these conditions.

formation, even after two hours. While the lack of activity data for these catalysts prevents a comparison between these catalyst deactivation modes, exposure of a ZN catalyst with an unknown level of deterioration to atmospheric pressures of ethylene at reaction temperature may constitute a simple diagnostic test to gauge catalyst deterioration. In contrast to the previous activity data from Table 1, these experiments show a greater sensitivity of the ZN catalyst system to reaction conditions, gas phase reactor at atmospheric ethylene pressure and without an organoaluminum scavenger. The reactivity observed in the slurry phase, in the presence of TEA and higher ethylene pressures, suggests that the deteriorated catalysts can be reactivated for polyethylene formation. However, the modifications to the catalyst surface still negatively affect the final polymer morphology with the presence of polyethylene threads.

4. Conclusions

The results from this study on modified ZN catalysts have revealed that specific environmental factors affect catalyst structure, reactivity, and final polymer morphology. Deteriorated catalysts were synthesized by single exposure of a pristine catalyst to extreme degradation conditions, e.g. dry air, heat, or moisture. The modified catalysts showed reduced HDPE activity with decreasing activity in the order: $C_{AsSuch} > C_{DryAir} > C_{Moisture} > C_{Heat}$. The modified catalysts also produced HDPE samples with polyethylene threads observed via SEM images and with undesirable morphologies. Sphericity measurements on the polymer powder was studied via image analysis and showed a decrease in ideal spherical morphology as $C_{AsSuch} > C_{Heat} > C_{Moisture} > C_{DryAir}$. Changes to polymer morphology are concerning as polyethylene threads can cause catastrophic reactor fouling and undesirable particle shapes influence polymer processing.

To predict the formation of polymer threads caused by catalyst degradation, spectroscopic characterization methods were used to gain insight on pristine and deteriorated ZN catalyst. Lewis acidity of the $MgCl_2$ support were analyzed using CO FT-IR and the oxidation state of Ti species determined using DR UV–Vis. These techniques were able to differentiate the effect of diverse environmental conditions causing catalyst deterioration. Exposure of the pristine catalyst to dry air oxidized half of the Ti species but caused minimal changes to the support in terms of CO FTIR. Exposing the pristine catalyst to an extreme heat treatment caused a decline in porosity and $MgCl_2$ Lewis acid sites but resulted in minimal Ti oxidation. Moisture caused complete oxidation of all Ti species, complete loss in porosity, eliminated $MgCl_2$ Lewis acid sites, and formed new structures related to TiO_2 and Al_2O_3. Surface area measurements also showed dramatic changes when comparing the different catalysts, unique to the type of environmental condition.

Polymer formation was monitored for C_{AsSuch} using DRIFTS at 358 K and 1 bar ethylene. The large band intensity at 1466 cm^{-1} confirms the formation of crystalline HDPE. A comparison between the initiating rate constant, $k_i = 0.147\ min^{-1}$, and the ethylene propagation rate constant, $k_p \geq 16.314\ min^{-1}$, reveal that propagation is at least 2 orders of magnitude faster. In contrast, the degraded catalysts showed no polymer activity. This suggests that deteriorated catalysts are reactivated in the slurry phase when exposed to organoaluminum scavengers and/or higher ethylene pressure.

Overall, these results show that diagnostic, spectroscopic techniques can be used to characterize and differentiate ZN catalysts exposed to environmental factors. Using simple analytical tests, catalyst structure might be analyzed to predict catalyst reactivity and the appearance of polymer threads. This suggests that these techniques are ideal for quality control testing to prevent economic losses at industrial facilities due to reactor fouling and poor HDPE properties from deteriorated catalysts. These results will have an important impact as industrial actors continue to operate ZN polyolefin production facilities.

Acknowledgment

This project received funding from Total Research and Technology Feluy. The authors would like to thank Silvia Zanoni and Marjolein Velthoen of Utrecht University and Dr. Alessandro Piovano of University of Torino for helpful discussion with the FT-IR and UV-Vis experiments.

Appendix A. Supplementary material

Supplementary data associated with this article can be found, in the online version, at https://doi.org/10.1016/j.jcat.2018.04.012.

References

[1] World Polyolefins Analysis, Chemical Market Associates, Inc., 2005.
[2] "Polyethylene Resins, High-Density (HDPE)" from Chemical Economics Handbook, IHS Markit, 2017.
[3] K. Ziegler, E. Holzkamp, H. Breil, H. Martin, Angew. Chem. In. Ed. 67 (1955) 426.
[4] L.L. Böhm, Angew. Chem. Int. Ed. 42 (2003) 5010.
[5] R. Mülhaupt, Macromol. Chem. Phys. 204 (2003) 289.
[6] E. Morra, E. Giamello, S. Doorslaer, G. Antinucci, M. D'Amore, V. Busico, M. Chiesa, Angew. Chem. Int. Ed. 54 (2015) 4857.
[7] E. Groppo, K. Seenivasan, C. Barzan, Catal. Sci. Technol. 3 (2013) 858.
[8] S.H. Kim, G.A. Somorjai, Proc. Natl. Acad. Sci. U.S.A. 103 (2006) 15289.
[9] Y.V. Kissin, J. Catal. 292 (2012) 188.
[10] J.R. Severn, J.C. Chadwick, R. Duchateau, N. Friederichs, Chem. Rev. 105 (2005) 4073.
[11] G. Fink, B. Steinmetz, J. Zechim, C. Pryzbyla, B. Tesche, Chem. Rev. 100 (2000) 1377.
[12] T.F. McKenna, J.B.P. Soares, Chem. Eng. Sci. 56 (2001) 3937.
[13] T.F. McKenna, A. Di Martino, G. Weickert, J.B.P. Soares, Macromol. React. Eng. 4 (2010) 40.
[14] A. Munoz-Escalona, J.G. Hernandez, J.A. Gallardo, J. Appl. Polym. Sci. 29 (1984) 1187.
[15] R. Rashedi, F. Sharif, Ind. Eng. Chem. Res. 53 (2014) 13543.
[16] F. Machado, E.L. Lima, J.C. Pinto, T.F. McKenna, Polym. Eng. Sci. 51 (2011) 302.
[17] S.D. Gray, T.J. Coffy, US Patent 6734134 B1, 2004, to Fina Technology, Inc.
[18] V.N. Panchenko, N.V. Semikolenova, I.G. Danilova, E.A. Paukshtis, V.A. Zakharov, J. Mole. Catal. A: Chem. 142 (1999) 27.
[19] M.E.Z. Velthoen, A. Muñoz-Murillo, A. Bouhmadi, M. Cecius, S. Diefenbach, B. M. Weckhuysen, Macromolecules 51 (2018) 343.
[20] A. Zecchina, C.O. Areàn, Chem. Soc. Rev. 25 (1996) 187.
[21] G. Ghiotti, E. Garrone, C. Morterra, F. Boccuzzi, J. Phys. Chem. 83 (1979) 2863.
[22] M. D'Amore, K.S. Thushara, A. Piovano, M. Causà, S. Bordiga, E. Groppo, ACS Catal. 6 (2016) 5786.
[23] J.H. Teuben, E.J.M. De Boer, A.H. Klazinga, E. Klei, J. Mol. Catal. 13 (1981) 107.
[24] A. Piovano, G.A. Martino, C. Bartzan, Rend. Fis. Acc. 28 (2017) 28.
[25] K.I. Hadjivanov, D.G. Klissurski, Chem. Soc. Rev. 25 (1996) 61.
[26] U. Diebold, Surf. Sci. Rep. 48 (2003) 53.
[27] N.B. Muddada, U. Olsbye, T. Fuglerud, S. Vidotto, A. Marsella, S. Bardiga, D. Gianolio, G. Leofanti, C. Lamberti, J. Catal. 284 (2011) 236.
[28] M. Wojdyr, J. Appl. Crystallogr. 43 (2010) 1126.
[29] D. Cicmil, J. Meeuwissen, A. Vantomme, I.K. Van Ravenhorst, H.E. Van Der Bij, A. Munoz-Murillo, B.M. Weckhuysen, Angew. Chem. Int. Ed. 54 (2015) 13073.
[30] J.J.H.B. Sattler, J. Ruiz-Martinez, E. Santillan-Jimenez, B.M. Weckhuysen, Chem. Rev. 114 (2014) 10613.
[31] K. Seenivasan, A. Sommazzi, F. Bonino, S. Bordiga, E. Groppo, Chem. Eur. J. 17 (2011) 8648.
[32] I. Pollini, Solid State Commun. 47 (1983) 403.
[33] C.H. Maulet, J.N. Tothill, P. Strange, J.A. Wilson, J. Phys. Chem. 21 (1988) 2153.
[34] H. Brintzinger, J. Am. Chem. Soc. 89 (1967) 6871.
[35] G.A. Nesterov, V.A. Zakharov, E.A. Paukshtis, E.N. Yurchenko, Y.I. Yermakov, Kinet. Catal. 20 (1979) 429.
[36] N.G. Maksimov, G.A. Nesterov, V.A. Zakharov, P.V. Stchastnev, V.F. Anufrienko, Y.I. Yermakov, J. Mol. Catal. 4 (1978) 167.
[37] C. Copéret, D.P. Estes, K. Larmier, K. Searles, Chem. Rev. 116 (2016) 8463.
[38] V.A. Zakharov, Y.A. Ryndin, J. Mol. Catal. 56 (1989) 183.
[39] O.A. Kholdeeva, T.A. Trubitsina, R.I. Maksimovskaya, A.V. Golovin, W.A. Neiwert, B.A. Kolesov, X. Lopez, J.M. Poblet, Inorg. Chem. 43 (2004) 2284.
[40] D. Cicmil, J. Meeuwissen, A. Vantomme, B.M. Weckhuysen, ChemCatChem 8 (2016) 1937.
[41] P. Cossee, J. Catal. 3 (1964) 80.
[42] E.J. Arlman, J. Catal. 3 (1964) 89.
[43] E.J. Arlman, P. Cossee, J. Catal. 3 (1964) 99.
[44] N.M. Doherty, J.E. Bercaw, J. Am. Chem. Soc. 107 (1985) 2670.
[45] P.J. Chirik, J.E. Bercaw, Organometallics 24 (2005) 5407.
[46] Y.V. Kissin, R.I. Mink, T.E. Nowlin, A.J. Brandolini, Top. Catal. 8 (1999) 69.
[47] D.K. Steelman, S. Xiong, P.D. Pletcher, E. Smith, J.M. Switzer, G.A. Medvedev, W. N. Delgass, J.M. Caruthers, M.M. Abu-Omar, J. Am. Chem. Soc. 135 (2013) 6280.
[48] P.D. Pletcher, J.M. Switzer, D.K. Steelman, G.A. Medvedev, W.N. Delgass, J.M. Caruthers, M.M. Abu-Omar, ACS Catal. 6 (2016) 5138.
[49] G.A.H. Nooijen, Eur. Polym. J. 30 (1994) 11.